SUPPLEMENTAL MATERIAL

Calculation method

The evolving mineralogy and bulk water content of each lithology was calculated along each of three example geotherms (after Syracuse et al., 2010), starting at 0.5 GPa and terminating at 6.5 GPa (at corresponding temperatures, see inset panels of Fig. 1). Calculations utilized Gibbs' energy minimization with Perple_X version 6.6.7 (Connolly, 2005). Each geotherm was discretized into approximately 2000 *P-T* points, with free energy minimizations (calculation of mineral assemblage, abundances and compositions) undertaken at each point. For calculations in Figure 1 of the paper (also shown below as bold curves in DR-2 and as panel 'a' of DR-3), the composition of any garnet and/or fluid produced at a *P-T* point was extracted from the bulk rock composition before proceeding to the next point.

Fluid was considered as a H_2O–CO_2 binary solution (Holland and Powell, 1991, 1998) but in practice was always strongly H_2O dominated. Solubility of additional components was not considered. End-member thermodynamic data was from Holland & Powell (2004 'ds5.5' update to the 1998 dataset). In addition to end-member phases (e.g. rutile, quartz and coesite), several mineral solution models were considered: ideal clinozosite–epidote (Holland et al., 1998); a regular clinochlore–amesite–daphnite–Al-free-chlorite–Mn-chlorite solution (Holland and Powell, 1998); a tremolite–ferro-tremolite–pargasite–tschermakite–glaucophane–riebekite amphibole solution (Dale et al., 2000; Dale et al., 2005); an asymmetric (Van Laar) calcite–magnesite–dolomite solution (Holland and Powell, 2003); an asymmetric diopside–jadeite–hedenbergite–acmite solution (Green et al., 2007); regular grossular–almandine–pyrope–spessartine–khoharite mixing in garnet (White et al., 2005); asymmetric muscovite–paragonite–margarite–celadonite–ferro-celadonite–ferro-muscovite and symmetric Fe–Mg–Mn–Fe^{3+}–Al chloritoid and carpholite solutions (all after Smye et al., 2010). Incorporation of stilpnomelane followed Massonne and Willner (2008).

Our calculations included the effects of garnet and water fractionation from the bulk rock system. Figure DR-2 shows an example of these effects. If garnet chemistry is not progressively removed, the proportions and compositions of predicted phases can be substantially modified (e.g. Dragovic et al., 2012; Gaidies et al., 2008; Konrad-Schmolke et al., 2005; Marmo et al., 2002) Specifically, the *apparent* amount of garnet growth at higher *P-T* increases, thereby changing the predicted water:garnet production ratio (figure DR-2). Garnet fractionation can also lead to increased stability and growth of key phases such as lawsonite (e.g. Dragovic et al., 2012), which will significantly modify the rock's subsequent H_2O budget (Clarke et al., 2006). A subtle but important consequence of progressively sequestering garnet's components is that, because the Fe^{3+} content of this garnet is low, the residual Fe^{2+}:Fe^{3+} ratio decreases dramatically with garnet growth (bottom panel of Figure DR-2). Calculations suggest that unless components from garnet are allowed to re-enter the reactive volume (e.g. by garnet resorption), high *P-T* phases must grow from an almost Fe^{2+}-free environment (excluding effects of redox reactions).

Figure DR-2 highlights another key difference between this and earlier studies, in which free water was not removed from the system as it is produced. In models where such 'pore fluids' are retained (e.g. the fine curves in Figure DR-2), this H_2O is available for reaction when the system reaches '2nd growth' lawsonite (which occurs because the subduction path dP/dT is steeper than that of lawsonite stability above ~ 2.5 GPa). The free water is consumed by lawsonite at this point, also at the expense of garnet (which contributes CaO, Al_2O_3 and SiO_2). If water were re-introduced into the system at those conditions (e.g. from other dehydrating assemblages) then such lawsonite growth would indeed be possible and the rock would effectively be partially 're-fertilized'. A better general model will include progressive removal of the locally-produced fluids, as we do here. This reduces the abundance of '2nd growth' lawsonite, which is limited instead by breakdown of the scant remaining unstable hydrous phases (e.g. epidote; Figure DR-3).

Bulk rock compositions

	Hydrated MORB	Average Pelite
SiO_2	43.47	58.94
TiO_2	1.06	0.74
Al_2O_3	14.74	16.32
Fe_2O_3	5.32	1.27
Na_2O	1.96	1.70
K_2O	0.53	3.48
FeO	3.78	5.15
MgO	6.32	2.58
CaO	12.22	1.07
MnO	0.16	0.10
H_2O	7.63	8.63
CO_2	2.80	-

Table DR1. *Initial bulk rock compositions used for calculations presented in manuscript (wt %). Hydrated MORB after Staudigel et al. (1996), with additional H_2O included to ensure fluid saturation at the 0.5 GPa initiation of the model. Pelite after Shaw (1956), with modifications from Mahar et al. (1997) and Caddick & Thompson (2008). Compositions used for figure 1 (and supplementary figure DR-3a) progressively deviate from these tabulations as garnet and/or fluid are produced and extracted.*

Starting bulk water content

One of the assumptions of our modeling was that the system passed through 0.5 GPa in a water saturated state. If the rock were not initially saturated, there would be less total dehydration flux. In fact, with much lower initial water, several early hydrous phases would be unstable and thermodynamic modeling predicts that garnet growth, marked by a distinctive Ca-Mn rich composition, could begin at much lower *P-T*, before significant fluid production. On the other hand, such dry low-*T* conditions could also lead to the persistence of metastable assemblages (e.g., Baxter 2003; Clarke et al. 2006), including overstepping and delay of this predicted low-*T* garnet

growth until kinetic barriers were overcome when water saturated conditions were met either by internally derived dehydration (i.e., where initial bulk water content intersects dashed curve in Fig. 1) or by external fluid infiltration. The data compilation by Hacker et al. (2003a) provides valuable context for the question of initial bulk water content. Their analysis shows that low grade zeolite, prehnite-pumpellyite-actinolite, and lawsonite-jadeite facies rocks contain high water contents, averaging between 4.4 and 5.8 wt% H_2O. These values are near water saturation for rocks entering the span of garnet growth in Figure 1 (where dashed curves effectively denote the fluid saturation surface). While the existence of very low *P-T*, high Mn–Ca garnet appears to be limited in nature (Hacker et al. 2003a), its rare occurrence (e.g., Pabst et al. 2012 report such garnets in ~350 °C blueschist clasts in serpentinite mud volcanoes), could be used to infer starting water content and dehydration timing.

Closed system assumption

In our model, we allow for the escape of a binary H_2O-CO_2 fluid produced at each model increment, and we treat the local fractionating effect of garnet growth on the surrounding reactive matrix. Otherwise, for simplicity, we assume that the bulk rock chemistry remains fixed throughout the model. However in natural systems, especially given the copious evidence (including our own modelling) for fluid production and metasomatism, some amount of open system chemical exchange is inevitable. Numerous studies have shown the potential for loss (or gain) of major elements (like Si, K, Na, Ca) trace elements (like Li, B) and their isotopes by interactions with these metasomatising fluids (e.g. Bebout, 1995; Breeding et al., 2003; John et al., 2012; Manning, 2004; Marschall et al., 2009; Zack and John, 2007). Furthermore, it has been shown that certain redox reactions (for example lawsonite breakdown) can produce free oxygen and an oxidizing fluid which leaves the residual rock system in a progressively more reduced (lower fO_2) state as that fluid is removed (e.g. Groppo and Castelli, 2010). Sensitivity analysis of such open system chemical exchange on the garnet:water production correlations we determine here will be worth exploring in future study. For now, we note the remarkable similarity between total water:garnet production ratios (well within a factor of ~4; see Figure 1) spanning extremely compositionally diverse end-members (MORB and pelite). This suggests that more subtle compositional variations due to open system metasomatism or initial protolith compositions will generally create only second order effects. The most significant of these effects would be those that permit stabilization (or destabilization) of a particularly hydrous phase (e.g. addition of more K_2O to the MORB will permit both enhanced stilpnomelane stability at low *P-T* and enhanced phengite stability at high *P-T*).

Mineral abbreviations, and compositions of hydrous phases

Anhydrous phase abbreviations: Calcite-dolomite (Cc), Coesite (Coe), Garnet (Gt), Kyanite (Ky), Omphacite (Omph), Quartz (Qtz), Rutile (Rut), Titanite (Sph). The purpose of the following list is to clarify the molar water contents of each phase considered in our calculations, so phases calculated as solid solutions are represented here by a single end-member.

Amphibole	(Amph):	$Na_2Mg_3Al_2Si_8O_{22}(OH)_2$
Carpholite	(Car):	$FeAl_2Si_2O_6(OH)_4$
Chlorite	(Chl):	$Mg_4Al_4Si_2O_{10}(OH)_8$
Chloritoid	(Ctd):	$FeAl_2SiO_5(OH)_2$
Epidote	(Ep):	$Ca_2FeAl_2Si_3O_{12}(OH)$
Lawsonite	(Law):	$CaAl_2Si_2O_7(OH)_2 \cdot H_2O$
Paragonite	(Parag):	$NaAl_3Si_3O_{10}(OH)_2$
Phengite	(Phen):	$KMgAlSi_4O_{10}(OH)_2$
Stilpnomelane	(Stlp):	$K_5Fe_{48}Al_5Si_{67}\ O_{168}(OH)_{48} \cdot (H_2O)_{36}$

Example reaction stoichiometries for Nicaragua geotherm

Below we show an example of the garnet forming dehydration reactions for MORB and pelite in the Nicaragua geotherm. Reactions are listed in units of moles consumed/produced per 100 kilograms of rock. Note that the molar water:garnet stoichiometric production ratios evident in the equations below can be re-cast (by considering rock and mineral molecular weights and densities) into the wt% water per vol% garnet units, as shown in Figure 1. These are the sum of all successive *changes* in phase assemblage in the garnet-growth interval, and do not directly reflect absolute phase abundance at the start or end of garnet growth (abundances are shown in Figure DR-3). "Overall" reactions correspond to the full garnet growth interval as shown in Figure 1. "Light gray" and "Dark Gray" correspond to discrete spans of garnet growth as shown in Figure 1.

Nicaragua MORB

Overall

37 Amph + 0.64 Stlp + 134 Lws + 13 Sph =
2.6 Cc + 4.2 Pheng + 170 Omph + 89 Qtz + 20 Ep + 79 Ky + 15 Rut + 32 Gt + 330 H_2O

Light Gray 1

9.0 Amph + 0.64 Stlp + 11 Lws + 13 Sph =
0.50 Cc + 3.3 Pheng + 6.3 Chl + 42 Omph + 36 Qtz + 14 Rut + 2.1 Gt + 40 H_2O

Dark Gray

48 Omph + 124 Lws + 6.3 Chl =
2.7 Cc + 63 Ep + 0.73 Pheng + 7.0 Amph + 48 Qtz + 0.90 Rut + 29 Gt + 229 H_2O

Light Gray 2

51 Ep + 0.59 Cc + 35 Amph =
0.17 Pheng + 176 Omph + 79 Ky + 4.8 Qtz + 0.20 Rut + 0.75 Gt + 60 H_2O

Since the 'overall' reaction is cumulative for a significant *P-T* span of garnet growth, phases that grow and then dissolve within this range (e.g. chlorite) may appear to be under represented. Table 2 summarizes the progressive storage and production of water for the Nicaragua MORB, cast in units of moles *of water* released or consumed by each phase per 100 kilograms of rock. This table thus excludes anhydrous phases, excepting garnet, which is shown for reference.

	Stlp	*Chl*	*Lws*	*Amph*	*Ep*	*Pheng*	*Water*	*Garnet*
Overall	***39***	***x***	***268***	***37***	***-10***	***-4***	***330***	***32***
Lt Gray 1	*39*	*-25*	*21*	*9*	*x*	*-3*	*40*	*2.1*
Dk Gray	*x*	*25*	*247*	*-7*	*-32*	*-1*	*229*	*29*
Lt Gray 2	*x*	*x*	*x*	*35*	*25*	*-<1*	*60*	*0.75*

Table DR2. *Water balance summary for Nicaragua MORB, presented as moles of water released (+) or consumed (-) by each phase per 100 kg of rock. Moles of garnet per 100 kg also shown for reference*

Nicaragua pelite

Overall

10 Amph + 0.39 Stlp + 19 Lws + 53 Carp =
11 Pheng + 25 Omph + 79 SiO_2 + 25 Ky + 0.50 Rut + 39 Gt + 166 H_2O

Light Gray 1

0.39 Stlp + 53 Carp + 36 Omph =
14 Amph + 6.9 Pheng + 1.1 Lws + 38 SiO_2 + 0.12 Rut + 2.4 Parag + 35 Ctd + 0.84 Gt + 67 H_2O

Dark Gray

25 Amph + 2.4 Parag + 35 Ctd + 20 Lws =
3.8 Pheng + 41 SiO_2 + 0.38 Rut + 25 Ky + 61 Omph + 38 Gt + 98 H_2O

	Stlp	*Carp*	*Amph*	*Lws*	*Ctd*	*Parag*	*Pheng*	*Water*	*Garnet*
Overall	***23***	***105***	***10***	***38***	***x***	***x***	***-11***	***166***	***39***
Lt Gray 1	*23*	*105*	*-15*	*-2*	*-35*	*-2*	*-7*	*67*	*0.84*
Dk Gray	*x*	*x*	*25*	*40*	*35*	*2*	*-4*	*98*	*38*

Table DR3. *Water balance summary for Nicaragua pelite, presented as moles of water released (+) or consumed (-) by each phase per 100 kg of rock. Moles of garnet per 100 kg also shown for reference*

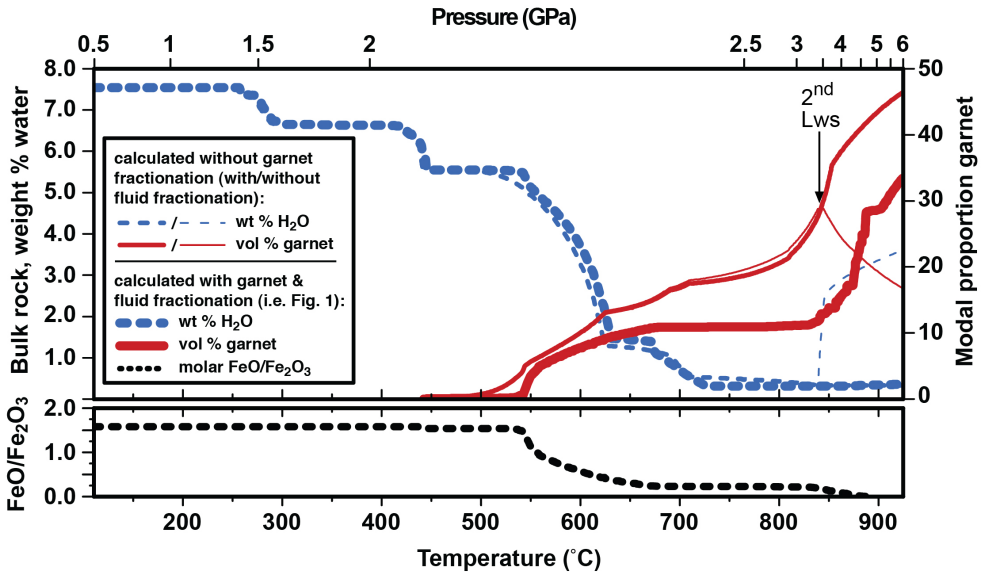

Data repository Figure DR1. *Diagram showing importance of garnet and water fractionation. Top panel shows progressive growth of garnet (in vol %) and production of water (in wt %) for hydrated MORB along the Nicaragua geotherm with garnet and water fractionation (bold lines, as in Figure 1), ignoring garnet fractionation (thinner lines), and ignoring both garnet and water fractionation (thinnest lines). Location of the apparent water increase at the second lawsonite-in reaction at ~3.5 GPa for the non-water fractionating model is indicated with an arrow. Note significant differences between the properly fractionated result and the other two. Lower panel shows the effect of garnet fractionation on the residual molar ferrous/ferric iron ratio.*

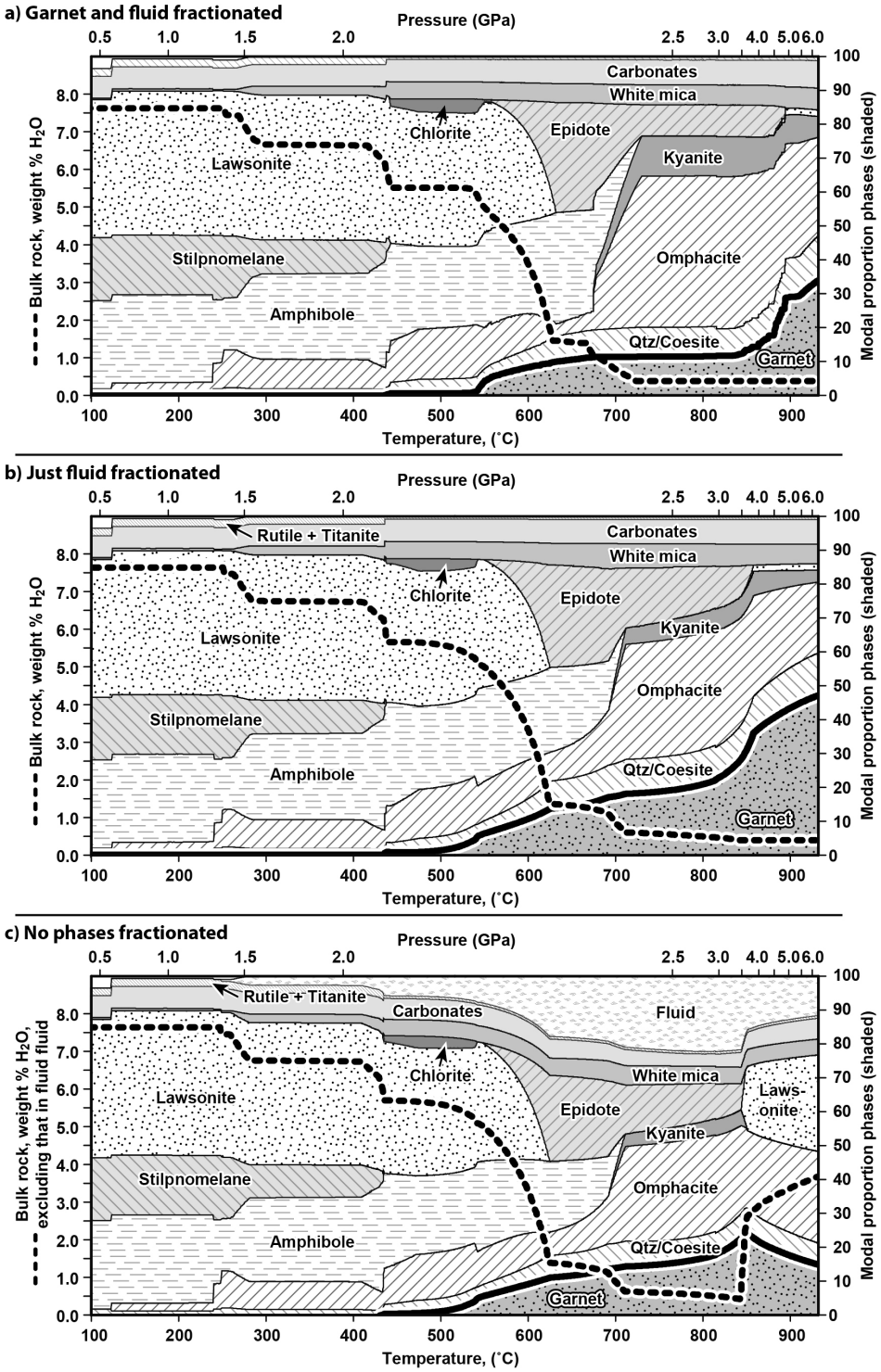

Figure DR2. *Phase abundances calculated for a hydrated MORB on the Nicaragua geotherm. Calculations involve different assumptions: (a) garnet and fluid are progressively fractionated from the bulk rock composition as they form, (b) fluid is fractionated but garnet is not, (c) no phases are fractionated. Bold curves highlight garnet abundance (right-hand axis), bold dashed curves denote amount of bulk rock H_2O (excluding in fluid). Option (a) as in Figure 1c. Note that in (c) the persistence of a fluid phase could also lead to wet-melting*

(Hermann and Green, 2001; Schmidt and Poli, 1998; Vielzeuf and Schmidt, 2001), which is not depicted here. Melt fraction would be proportional to H_2O content. Thermodynamic data for many of the lower temperature (<400 ˚C) phases includes greater uncertainties, though the first-order phase petrology should still be accurate for the bulk composition modeled. For example, the dominance of stilpnomelane over chlorite at lower P-T is due to the presence of a small amount of potassium, which stabilizes stilpnomelane (sequestering 96 moles of FeO + MgO, 134 moles of SiO_2 and 120 moles of H_2O per 5 moles of K_2O, and destabilizing chlorite accordingly). Low T stability of amphibole and pyroxene is partly also a consequence of this, and dominance of the thermodynamics of the diopside end-member. Fortunately, these uncertainties manifest themselves most strongly at temperatures below the bulk of garnet growth and are thus less relevant to the aims and key conclusions of this study.

References cited in supplementary material

Bebout, G. E., 1995, The impact of subduction-zone metamorphism on mantle-ocean chemical cycling: Chemical Geology, v. 126, no. 2, p. 191-218.

Breeding, C. M., Ague, J. J., Bröcker, M., and Bolton, E. W., 2003, Blueschist preservation in a retrograded, high-pressure, low-temperature metamorphic terrane, Tinos, Greece: Implications for fluid flow paths in subduction zones: Geochemistry Geophysics Geosystems, v. 4.

Caddick, M. J., and Thompson, A. B., 2008, Quantifying the tectono-metamorphic evolution of pelitic rocks from a wide range of tectonic settings: Mineral compositions in equilibrium: Contributions to Mineralogy and Petrology, v. 156, p. 177-195.

Clarke, G. L., Powell, R., and Fitzherbert, J. A., 2006, The lawsonite paradox: a comparison of field evidence and mineral equilibria modelling Journal of Metamorphic Geology, v. 24, p. 715-725.

Connolly, J. A. D., 2005, Computation of phase equilibria by linear programming: A tool for geodynamic modeling and its application to subduction zone decarbonation: Earth and Planetary Science Letters, v. 236, p. 524-541.

Dale, J., Holland, T. J. B., and Powell, R., 2000, Hornblende-garnet-plagioclase thermobarometry: a natural assemblage calibration of the thermodynamics of: Contributions to Mineralogy and Petrology, v. 140, no. 3, p. 353-362.

Dale, J., Powell, R., White, R. W., Elmer, F. L., and Holland, T. J. B., 2005, A thermodynamic model for Ca-Na clinoamphiboles in Na_2O-CaO-FeO-MgO-Al_2O_3-SiO_2-H_2O-O: Journal of Metamorphic Geology, v. 23, p. 771-791.

Dragovic, B., Samanta, L. M., Baxter, E. F., and Selverstone, J., 2012, Using garnet to constrain the duration and rate of water-releasing metamorphic reactions during subduction: An example from Sifnos, Greece: Chemical Geology, v. 314, p. 9-22.

Gaidies, F., De Capitani, C., and Abart, R., 2008, THERIA_G: a software program to numerically model prograde garnet growth: Contributions to Mineralogy and Petrology, v. 155, p. 657-671.

Green, E., Holland, T. J. B., and Powell, R., 2007, An order-disorder model for omphacitic pyroxenes in the system jadeite-diopside-hedenbergite-acmite, with applications to eclogitic rocks: American Mineralogist, v. 92, p. 1181-1189.

Groppo, C., and Castelli, D., 2010, Prograde P–T Evolution of a Lawsonite Eclogite from the Monviso Meta-ophiolite (Western Alps): Dehydration and Redox Reactions during Subduction of Oceanic FeTi-oxide Gabbro: Journal of Petrology, v. 51, p. 2489-2514.

Hermann, J., and Green, D. H., 2001, Experimental constraints on high pressure melting in subducted crust: Earth and Planetary Science Letters, v. 188, p. 149-168.

Holland, T. J. B., Baker, J., and Powell, R., 1998, Mixing properties and activity-composition relationships of chlorites in the system $MgO–FeO–Al_2O_3–SiO_2–H_2O$: European Journal of Mineralogy, v. 10, p. 395-406.

Holland, T. J. B., and Powell, R., 1991, A Compensated-Redlich-Kwong (CORK) equation for volumes and fugacities of CO_2 and H_2O in the range 1 bar to 50 kbar and 100–1600 ˚C: Contributions to Mineralogy and Petrology, v. 109, p. 265-273.

-, 1998, An internally consistent thermodynamic data set for phases of petrological interest: Journal of Metamorphic Geology, v. 16, p. 309-343.

-, 2003, Activity-composition relations for phases in petrological calculations: an asymmetric multicomponent formulation: Contributions to Mineralogy and Petrology, v. 145, p. 492-501.

John, T., Gussone, N., Podladchikov, Y. Y., Bebout, G. E., Dohmen, R., Halama, R., Klemd, R., Magna, T., and Seitz, H.-M., 2012, Volcanic arcs fed by rapid pulsed fluid flow through subducting slabs: Nature Geosciences, v. 5, no. 7, p. 489-492.

Konrad-Schmolke, M., Handy, M. R., Babist, J., and O'Brien, P. J., 2005, Thermodynamic modelling of diffusion-controlled garnet growth: Contributions to Mineralogy and Petrology, v. 149, no. 2, p. 181-195.

Mahar, E., Powell, R., Holland, T. J. B., and Howell, N., 1997, The effect of Mn on mineral stability in metapelites: Journal of Metamorphic Geology, v. 15, no. 2, p. 223-238.

Manning, C. E., 2004, The chemistry of subduction-zone fluids: Earth and Planetary Science Letters, v. 223, p. 1-16.

Marmo, B. A., Clarke, G. L., and Powell, R., 2002, Fractionation of bulk rock composition due to porphyroblast growth: effects on eclogite facies mineral equilibria, Pam Peninsula, New Caledonia: Journal of Metamorphic Geology, v. 20, p. 151-165.

Marschall, H. R., Altherr, R., Gmeling, K., and Kasztovszky, Z., 2009, Lithium, boron and chlorine as tracers for metasomatism in high-pressure metamorphic rocks: a case study from Syros (Greece): Mineralogy and Petrology, v. 95, no. 3-4, p. 291-302.

Massonne, H. J., and Willner, A. P., 2008, Phase relations and dehydration behaviour of psammopelite and mid-ocean ridge basalt at very-low-grade to low-grade metamorphic conditions: European Journal of Mineralogy, v. 20, no. 5, p. 867 - 879.

Schmidt, M. W., and Poli, S., 1998, Experimentally based water budgets for dehydrating slabs and consequences for arc magma generation: Earth and Planetary Science Letters, v. 163, p. 361-379.

Shaw, D. M., 1956, Geochemistry of pelitic rocks. Part iii: major elements and general geochemistry: Bulletin of the Geological Society of America, v. 67, p. 919-934.

Smye, A. J., Greenwood, L. V., and Holland, T. J. B., 2010, Garnet–chloritoid–kyanite assemblages: eclogite facies indicators of subduction constraints in orogenic belts: Journal of Metamorphic Geology, v. 28, p. 753-768.

Staudigel, H., Plank, T., White, B., and Schmincke, H.-U., 1996, Geochemical fluxes during seafloor alteration of the basaltic upper oceanic crust: DSDP Sites 417 and418, Subduction: Top to Bottom: American Geophyiscal Union, p. 19-38.

Syracuse, E. M., van Keken, P. E., and Abers, G. A., 2010, The global range of subduction zone thermal models: Physics of the Earth and Planetary Interiors, v. 183, no. 1-2, p. 73-90.

Vielzeuf, D., and Schmidt, M. W., 2001, Melting relations in hydrous systems revisited: application to metapelites, metagreywackes and metabasalts: Contributions to Mineralogy and Petrology, v. 141, p. 251-267.

White, R. W., Pomroy, N. E., and Powell, R., 2005, An in situ metatexite–diatexite transition in upper amphibolite facies rocks from Broken Hill, Australia: Journal of Metamorphic Geology, v. 23, p. 579–602.

Zack, T., and John, T., 2007, An evaluation of reactive fluid flow and trace element mobility in subducting slabs: Chemical Geology, v. 239, no. 3-4, p. 199-216.